



# FeRA: Frequency-Energy Constrained Routing for Effective Diffusion Adaptation Fine-Tuning

Bo Yin<sup>1</sup> Xiaobin Hu<sup>1\*</sup> Xingyu Zhou<sup>2</sup> Peng-Tao Jiang<sup>3</sup> Yue Liao<sup>1</sup>

Junwei Zhu<sup>4</sup> Jiangning Zhang<sup>6</sup> Ying Tai<sup>5</sup> Chengjie Wang<sup>7</sup> Shuicheng Yan<sup>1</sup>

<sup>1</sup>National University of Singapore <sup>2</sup>University of Electronic Science and Technology of China <sup>3</sup>vivo <sup>4</sup>Tencent YouTu Lab  
<sup>5</sup>Nanjing University <sup>6</sup>Zhejiang University <sup>7</sup>Shanghai Jiao Tong University

## Abstract

Diffusion models have achieved remarkable success in generative modeling, yet how to effectively adapting large pre-trained models to new tasks remains challenging. We revisit the reconstruction behavior of diffusion models during denoising to unveil the underlying frequency–energy mechanism governing this process. Building upon this observation, we propose **FeRA**, a frequency-driven fine-tuning framework that aligns parameter updates with the intrinsic frequency–energy progression of diffusion. FeRA establishes a comprehensive frequency–energy framework for effective diffusion adaptation fine-tuning, comprising three synergistic components: (i) a compact frequency–energy indicator that characterizes the latent’s bandwise energy distribution, (ii) a soft frequency router that adaptively fuses multiple frequency-specific adapter experts, and (iii) a frequency–energy consistency regularization that stabilizes diffusion optimization and ensures coherent adaptation across bands. Routing operates in both training and inference, with inference-time routing dynamically determined by the latent frequency energy. It integrates seamlessly with adapter-based tuning schemes and generalizes well across diffusion backbones and resolutions. By aligning adaptation with the frequency–energy mechanism, **FeRA** provides a simple, stable, and compatible paradigm for effective and robust diffusion model adaptation. The code will be available: <https://github.com/YinBo0927/FeRA.git>.

## 1. Introduction

Diffusion models have fundamentally reshaped generative modeling [13, 17, 19, 36]. Advances in denoising-based likelihood learning, consistency training, and distillation have stabilized optimization and accelerated sampling [13, 18, 39, 44, 51], while the shift from compact U-Nets to

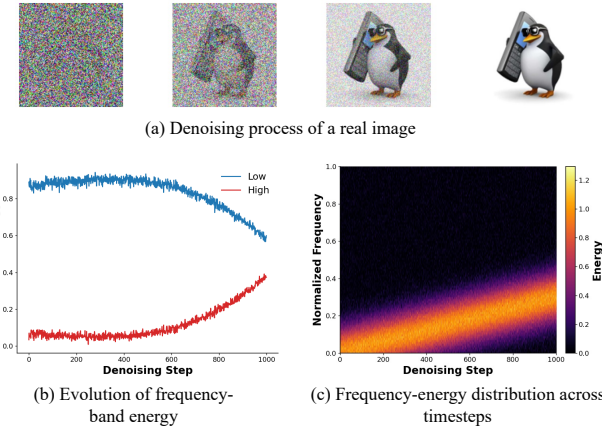


Figure 1. Frequency-energy evolution during denoising. (a) Visualization of the denoising process. (b) Evolution of frequency-band energies. (c) Frequency-energy distribution across timesteps.

cross-scale attention with strong semantic encoders has improved resolution and alignment [33, 36]. Beyond generic image synthesis, diffusion models now power personalization, editing and controllable generation [9, 31, 38, 56]. Open frameworks such as Stable Diffusion [36] bridge research and deployment, making it feasible and increasingly essential to adapt large pretrained backbones to new tasks without harming generalization. This motivates a central challenge: how to efficiently and reliably adapt powerful diffusion models to diverse downstream scenarios within limited computational and storage budgets, placing parameter-efficient fine-tuning (PEFT) [15, 29] at the center of attention.

The research trajectory of PEFT has generally followed three main routes in Fig. 2: **1) Additive methods** attach external adapters or side branches, which are simple to train but increase inference overhead [14, 29]. **2) Reparameterization methods**, such as low-rank decomposition, embed learnable updates into the original weights for seamless merging at inference [15]. **3) Selective methods** tune only a small subset of parameters or channels, preserving

\*Corresponding authors.

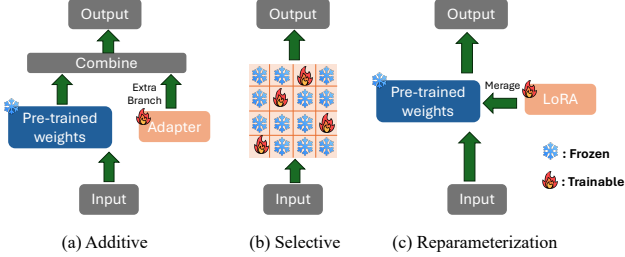


Figure 2. The classical parameter-efficient fine-tuning methods.

pretrained priors but increasing implementation complexity [11]. These existing fine-tuning paradigms, including additive, reparameterization, and selective methods, still face inherent limitations. These methods uniformly handle noise across all timesteps. However, diffusion denoising is inherently stage-varying, where the model exhibits distinct noise-signal characteristics over time [6, 13, 20, 30], as shown in Fig. 1. Consequently, such uniform adaptation fails to align with the intrinsic noise-dependent dynamics of the diffusion process. This raises a fundamental question: *Can we design a fine-tuning strategy that adapts to the varying noise conditions throughout the diffusion process rather than enforcing uniform updates across all timesteps?*

Given the stage-varying nature of diffusion denoising, a dynamic adaptation mechanism across timesteps naturally becomes desirable. Such dynamic capacity can, in principle, be achieved through mixture-of-experts (MoE) mechanisms. Inspired by the success of MoE architectures, recent studies attempt to address this limitation by introducing dynamic routing mechanisms that selectively activate different experts across timesteps or layers. Such designs provide adaptive capacity and improve specialization, yet most routing keys remain discrete and are typically driven by timestep or structural index, which often leads to unstable optimization and limited generalization across diffusion backbones. To move beyond these discrete and task-specific schemes, we explore *whether the routing process itself can be guided by the continuous pattern observed in diffusion denoising rather than by manually defined timestep indices, thereby enabling fine-tuning to follow the model’s inherent denoising progression.*

Therefore, we propose **FeRA**, a frequency-energy-driven framework for parameter-efficient fine-tuning. FeRA employs frequency experts that reflect the frequency-energy progression observed in diffusion denoising. At each step, the latent representation is decomposed into distinct frequency bands, and their energy proportions are fed into a frequency router to produce continuous routing weights. These weights softly blend the frequency experts, enabling the model to adapt smoothly across energy domains while preserving pretrained priors. To further stabilize training, a frequency-consistency regularization constrains the dis-

crepancy of update magnitudes between adjacent bands. The unified routing and regularization generalize across model scales and configurations, providing a stable, transferable, and lightweight paradigm for energy-aware fine-tuning. The main contributions of this work are as follows:

- **Frequency-energy analysis of diffusion denoising.** We reveal a consistent coarse-to-fine progression that links denoising steps to frequency-energy composition.
- **Frequency-driven routing architecture (FeRA).** We propose a Frequency Energy Indicator to characterize the frequency-energy evolution across timesteps, and leverage it to guide a soft frequency-based expert routing mechanism that replaces discrete timestep hard routing.
- **Frequency-energy consistency regularization.** We introduce a lightweight frequency-energy-based regularization that stabilizes training and enhances the transferability of efficient diffusion adaptation.
- **Comprehensive experimental validation.** We conduct extensive experiments across diverse datasets and diffusion backbones, demonstrating consistent improvements in generation quality and generalization, validating the effectiveness of our frequency-driven design.

## 2. Related Work

### 2.1. Diffusion Models

Diffusion models [13, 30, 43] have achieved remarkable success in generative modeling by progressively denoising Gaussian noise into structured images. Latent diffusion [36] further improves efficiency by operating in a compressed latent space, enabling large-scale text-to-image generation exemplified by Stable Diffusion. Subsequent research has extended diffusion models to a wide range of applications, including conditional generation [29, 53, 56], controllable synthesis [45, 46], video generation [4, 12], 3D content creation [31, 50], and audio-visual modeling [32, 42]. Beyond applications, several studies investigate the theoretical and structural properties of diffusion processes, such as noise scheduling [20, 40], consistency training [44], and frequency-domain analysis [24]. These works collectively reveal that diffusion denoising proceeds in a coarse-to-fine manner, where low-frequency structures form before high-frequency details, providing new insights for enhancing generative quality and interpretability.

### 2.2. PEFT for Generative Models

Parameter-efficient fine-tuning (PEFT) techniques have become essential for adapting large diffusion models to new concepts or domains without full retraining [5, 27]. Early approaches such as Textual Inversion [9] and Dream-Booth [38] personalize models by learning small embeddings or tuning only a subset of parameters. LoRA [15] introduces low-rank adaptation and has been widely adopted

in diffusion frameworks for its efficiency and scalability [57]. Extensions including ControlNet [56], T2I-Adapter [29], and IP-Adapter [53] integrate auxiliary networks to enhance conditional control, while adapter fusion and expert routing [23, 58] further improve flexibility and robustness. More recent studies investigate unified and task-aware PEFT architectures [16, 54], reflecting a growing interest in scalable and modular adaptation for large generative models. Despite differences in structure and application, these methods share a common objective: to enable controllable and data-efficient fine-tuning, yet they implicitly assume isotropic denoising dynamics and overlook the timestep-wise anisotropy of diffusion reconstruction.

### 2.3. Mixture of Expert

Mixture-of-Experts (MoE) architectures introduce conditional computation by activating different parameter subsets based on input features or contextual cues [7, 41, 48]. This paradigm improves model capacity and specialization without linearly increasing inference cost. Recent works extend MoE to vision and generative tasks, where expert routing is driven by spatial location, semantic content, or timestep signals [10, 10]. In diffusion models, MoE-based adapters or routers have been explored to decouple timestep-dependent behaviors [26, 35, 58], allowing distinct experts to handle different denoising stages. However, most of these methods rely on discrete timestep gating, which introduces hard boundaries and unstable expert activation during training.

## 3. Frequency-Energy in Denoising

A diffusion model gradually transforms Gaussian noise into a structured image through iterative denoising [13, 47, 52, 55]. As illustrated in Fig. 1(a), this process exhibits a clear visual transition from chaotic noise to coherent structure. To analyze this progression quantitatively, we compute the 2D Fourier amplitude spectrum  $A_t(f)$  of each intermediate image  $x_t$ . By integrating spectral energy within predefined low- and high-frequency bands, we obtain their normalized evolution over timesteps (Fig. 1(b)). The results reveal a consistent shift of energy dominance from low to high frequencies as denoising proceeds. The frequency-energy distribution in Fig. 1(c) further confirms that high-frequency components only become prominent in later stages, indicating that diffusion reconstruction progressively shifts energy from low to high frequencies.

This behavior can be explained through the frequency-dependent signal-to-noise ratio (SNR) of the diffusion process [1]. Given the forward formulation  $x_t = \sqrt{\alpha_t} x_0 + \sqrt{1 - \alpha_t} \epsilon$ , its Fourier-domain representation is

$$\hat{x}_t(f) = \sqrt{\alpha_t} \hat{x}_0(f) + \sqrt{1 - \alpha_t} \hat{\epsilon}(f). \quad (1)$$

The per-frequency SNR is defined as

$$\text{SNR}_t(f) = \frac{\alpha_t |\hat{x}_0(f)|^2}{(1 - \alpha_t) \mathbb{E}[|\hat{\epsilon}(f)|^2]} \propto \frac{\alpha_t}{(1 - \alpha_t) f^\gamma}, \quad (2)$$

since natural images approximately follow a power-law spectrum  $|\hat{x}_0(f)|^2 \propto 1/f^\gamma$  with  $\gamma \approx 2$  [8, 37], implying that low frequencies carry substantially higher energy than high frequencies and we note that the denominator  $\mathbb{E}[|\hat{\epsilon}(f)|^2]$  remains nearly constant across frequencies, so the frequency dependence of  $\text{SNR}_t(f)$  primarily arises from the signal term. This relation indicates that both smaller  $\alpha_t$  and higher  $f$  lead to rapidly diminishing SNR. When  $\alpha_t$  is small at early timesteps, the signal term  $|\hat{x}_0(f)|^2$  becomes negligible compared to the noise power. This effect is particularly pronounced at high frequencies, where the intrinsic decay  $|\hat{x}_0(f)|^2 \propto 1/f^\gamma$  further suppresses the signal energy. As a result, the observed spectrum  $\hat{x}_t(f)$  in these bands is effectively noise-dominated and contains almost no recoverable structure. In contrast, low-frequency components maintain substantially higher SNR, allowing coarse spatial layouts to remain statistically discernible even in the early stages of denoising. As  $\alpha_t$  increases over time, the effective SNR of high-frequency bands gradually improves, enabling the model to recover fine-grained details in later denoising steps.

Since the VAE encoder  $\mathcal{E}$  is locally approximately linear within the manifold of natural images [3, 21, 36], its latent representation  $z_t = \mathcal{E}(x_t)$  satisfies  $\hat{z}_t(f) \approx H(f) \hat{x}_t(f)$ , where  $H(f)$  denotes the encoder's local frequency response that approximately preserves the spectral structure of natural images, leading to a matching latent SNR,  $\text{SNR}_t^{(z)}(f) \approx \text{SNR}_t(f)$ . Hence, the same evolution persists within the latent domain, where we later define our frequency indicators and routing strategy, ensuring that the model's adaptive behavior remains aligned with the underlying spectral progression throughout the entire denoising trajectory.

## 4. Frequency-Energy Constrained Routing

Motivated by the frequency-energy analysis in Section 3, we propose **FeRA**, a parameter-efficient fine-tuning framework that introduces frequency-energy-aware mechanisms at both architectural and training levels. As illustrated in Fig. 3, FeRA first employs a Difference-of-Gaussians (DoG) [28] operator to extract the relative energy distribution across different frequency bands, forming a compact *Frequency-Energy Indicator (FEI)* that characterizes the latent's frequency-energy state. The FEI is then fed into a *Soft Frequency Router*, which adaptively blends multiple LoRA experts according to the current frequency-energy composition, providing a continuous and interpretable alternative to timestep-based hard routing. To further ensure consistency during training, FeRA incorporates a *Frequency-*

*Energy Consistency Loss (FECL)* that aligns the denoising trajectory with the inherent frequency-energy evolution.

#### 4.1. Frequency-Energy Indicator (FEI)

We define a simple descriptor that summarizes the frequency-energy of the latent feature  $z_t \in \mathbb{R}^{C \times H \times W}$  at denoising step  $t$ . Let  $G_\sigma$  be a Gaussian blur with standard deviation  $\sigma$  measured in latent pixels. In the frequency domain with radial frequency  $\rho$ , its response is  $\hat{G}_\sigma(\rho) = e^{-2\pi^2\sigma^2\rho^2}$ . A Difference-of-Gaussians (DoG)  $D_{\sigma_i, \sigma_j} = G_{\sigma_i} - G_{\sigma_j}$  is therefore a band-pass filter with response  $e^{-2\pi^2\sigma_i^2\rho^2} - e^{-2\pi^2\sigma_j^2\rho^2}$ , which is small near  $\rho = 0$  and at high  $\rho$ , and peaks at a middle range. Using  $n$  Gaussian kernels with scales  $\{\sigma_1, \dots, \sigma_n\}$  in a geometric progression (we use  $\sigma_k = \kappa \cdot 2^{k-1}$  for  $k = 1, \dots, n$ , with  $\kappa = \min(H, W)/128$ , implicitly corresponding to increasing frequency cutoffs), we construct  $n$  frequency bands. The filtered components are computed as follows:

$$z_t^{(k)} = \begin{cases} G_{\sigma_k} * z_t & \text{if } k = 1, \\ (G_{\sigma_k} - G_{\sigma_{k-1}}) * z_t & \text{if } 1 < k < n, \\ (\mathbb{I} - G_{\sigma_{n-1}}) * z_t & \text{if } k = n, \end{cases} \quad (3)$$

where  $G_{\sigma_k}$  denotes a Gaussian blur with standard deviation  $\sigma_k$ , and  $*$  is depth-wise convolution. We measure the energy of each band as:

$$E_t^{(k)} = \|z_t^{(k)}\|_2^2 = \sum_{c=1}^C \sum_{x=1}^H \sum_{y=1}^W \left( z_{t,c}^{(k)}(x, y) \right)^2, \quad k = 1, \dots, n. \quad (4)$$

By Parseval’s theorem [22], the spatial-domain per-band energy  $E_t^{(k)}$  equals its frequency-domain counterpart. Hence, the computed per-band quantity  $E_t^{(k)}$  is exactly the frequency-domain energy of  $z_t^{(k)}$ . With the dyadic spacing above, the filters exhibit minimal overlap and cover the full frequency spectrum, such that  $\sum_{k=1}^n E_t^{(k)} \approx \|z_t\|_2^2$ . We define the **Frequency-Energy Indicator (FEI)** as the normalized energy vector:

$$\mathbf{e}_t = \frac{[E_t^{(1)}, \dots, E_t^{(n)}]^\top}{\sum_{k=1}^n E_t^{(k)}} \in \mathbb{R}^n, \quad (5)$$

Which lies on the probability simplex and is invariant to global rescaling of  $z_t$ , offering a stable descriptor.

#### 4.2. Soft Frequency Router

Building upon FEI, we introduce a **Frequency-Aware Routing** mechanism that dynamically blends multiple LoRA experts according to the latent’s spectral state. Specifically, the FEI is projected through a lightweight MLP router  $g_\phi$  to produce  $M$  routing logits and weights:

$$\alpha_t = \text{softmax} \left( \frac{g_\phi(\mathbf{e}_t)}{\tau} \right) \in \mathbb{R}^M \quad (6)$$

where  $\mathbf{e}_t$  is FEI,  $\tau$  controls routing softness, and  $\alpha_{t,m}$  is the weight assigned to expert  $\mathcal{E}_k$ . The routed adapter output is the weighted mixture

$$y_t = \sum_{m=1}^M \alpha_{t,m} \mathcal{E}_m(z_t) \quad (7)$$

enabling smooth transitions across different frequency experts as the energy distribution evolves. This frequency-driven formulation improves continuity and interpretability over timestep-based hard gating. In practice we attach the frequency-energy experts to the same layers, use a small two-layer router, and fix  $\tau=0.7$ .

#### 4.3. Frequency-Energy Consistency Loss (FECL)

While the frequency router adaptively adjusts the contribution of LoRA experts, it does not explicitly regularize the spectral behavior of the latent representation. To enforce a consistent evolution of frequency energy during denoising, we introduce a **Frequency-Energy Consistency Loss (FECL)** applied in the latent space.

Let the latent predicted by the base model be  $z_t^{\text{base}}$  and the one adapted by LoRA be  $z_t^{\text{lora}}$ . We define the correction and reconstruction errors as

$$\delta_t = z_t^{\text{lora}} - z_t^{\text{base}}, \quad r_t = z_t^{\text{lora}} - z_t, \quad (8)$$

where  $z_t$  is the ground-truth latent at step  $t$ . Using the  $n$ -band decomposition from Sec. 4.1, we apply DoG filters  $D_{\sigma_{k-1}, \sigma_k}$  to obtain bandwise components:

$$\left( \delta_t^{(1)}, \dots, \delta_t^{(n)} \right) = D(\delta_t), \quad \left( r_t^{(1)}, \dots, r_t^{(n)} \right) = D(r_t), \quad (9)$$

where  $\delta_t = z_t^{\text{lora}} - z_t^{\text{base}}$  and  $r_t = z_t^{\text{lora}} - z_t$  denote the adapter correction and residual error, respectively. We then align the correction with the residual in the frequency domain via the **Frequency-Energy Consistency Loss (FECL)**:

$$\mathcal{L}_{\text{FECL}} = \sum_{k=1}^n w_k(t) \left( \frac{\|\delta_t^{(k)}\|_2}{\|\delta_t\|_2} - \frac{\|r_t^{(k)}\|_2}{\|r_t\|_2} \right)^2 \quad (10)$$

where  $w_k(t)$  are frequency-band weights derived from the current FEI (we use  $w_k(t) = \tilde{E}_t^{(k)} / \sum_j \tilde{E}_t^{(j)}$ ). The full objective is

$$\mathcal{L} = \mathcal{L}_{\text{denoise}} + \lambda_f \mathcal{L}_{\text{FECL}}. \quad (11)$$

Minimizing  $\mathcal{L}_{\text{FECL}}$  enforces *frequency-energy alignment* between the adapter correction and the residual across frequencies, concentrating updates where residual energy is present and suppressing updates where it is negligible.

## 5. Experiment

To validate the effectiveness of our method, we conduct experiments on two representative scenarios: downstream dataset fine-tuning and image customization. Specifically, we set the number of FEI and LoRA experts to

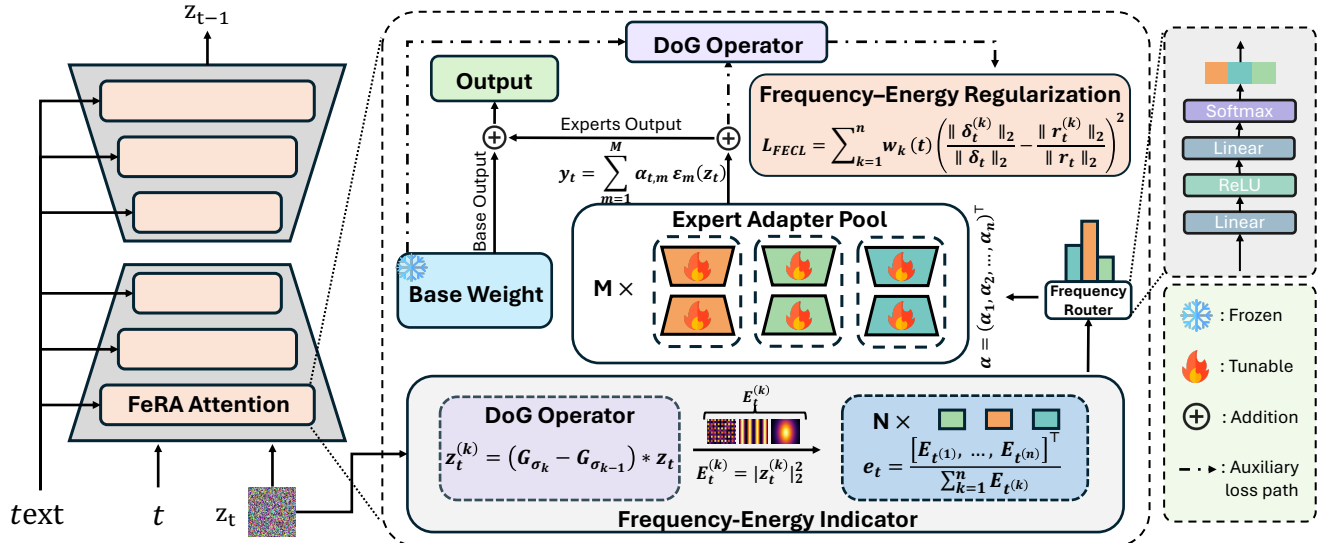


Figure 3. Overview of the FeRA framework. The **Frequency-Energy Indicator** (FEI) extracted by DoG operators guides a **Soft Frequency Router** to adaptively blend multiple LoRA experts. A **Frequency-Energy Consistency Loss** (FECL) further regularizes the spectral alignment between correction and residual during fine-tuning.

3, and why we set this number will be discussed in Section 5.3. We compare our approach with four state-of-the-art parameter-efficient fine-tuning methods: LoRA [15], DoRA [25] AdaLoRA [57], and SaRA [16], along with the full-parameter fine-tuning baseline. All models are fine-tuned under same training configurations for comparison.

## 5.1. Text-to-Image Style Adaptation

**Experiment Setting.** In this experiment, we fine-tune on five widely used CIVITAI style datasets, including Barbie Style, Cyberpunk Style, Elementfire Style, Expedition Style, and Hornify Style. We compare parameter-efficient fine-tuning methods on Stable Diffusion 2.0, 3.0 and FLUX.1 under three trainable parameter budgets of 5M, 20M, and 50M. More backbones can be found in Appendix. Results on additional backbones following the same protocol are provided in the Appendix. Each fine-tuned model is evaluated using three metrics: Fréchet Inception Distance (FID), CLIP Score, and Style Score for perceptual style consistency. The Style Score is obtained through a multimodal large language model (MLLM)-based quantitative evaluation using Qwen2.5-VL-7B-Instruct [2].

**Result Analysis.** The quantitative results are reported in Tab. 1. 1). Across SD 2.0, 3.0 and FLUX1., FeRA consistently ranks among the top-performing methods across most styles, achieving lower FID while maintaining competitive CLIP and Style scores. Even under the 5M budget, it attains the lowest FID on several datasets without compromising alignment. 2). As the trainable budget increases to 20M and 50M, FeRA captures finer stylistic details, with FID

continuing to improve and Style scores remaining stable, indicating that frequency-energy-aware soft routing scales effectively with model capacity rather than overfitting. 3). The full-parameter baseline is not uniformly dominant under these settings, while FeRA achieves comparable or better performance with substantially fewer parameters. Qualitative comparisons in Fig. 4 further shows coherent structure, accurate alignment, and high-fidelity style renderings.

## 5.2. Image Customization

**Experiment Setting.** We evaluate the proposed FeRA framework on personalized image generation, a representative task that tests a model’s ability to adapt to novel identities or concepts with limited examples. Specifically, we conduct experiments on five representative subject categories, including dog, clock, backpack, toy duck, and teapot. Following the standard DreamBooth protocol [38], we fine-tune a pre-trained Stable Diffusion 2.0 model using a small number of instance images (3-5) per subject, binding each identity to a unique rare token. All competing methods are implemented on the same UNet backbone for a fair comparison, including full finetuning, LoRA [15], DoRA [25], AdaLoRA [57], and SaRA [16]. For quantitative evaluation, we use CLIP-based similarity metrics [34] to measure both image-text alignment and visual fidelity, reporting CLIP-IMG and CLIP-Text scores, where higher values indicate better consistency between generated results and target identity descriptions.

**Result Analysis.** As summarized in Tab. 2, FeRA consistently achieves the highest or second-highest scores on

Table 1. Comparison with different parameter-efficient fine-tuning methods on Stable Diffusion 2.0, 3.0 and FLUX.1. **Orange bold** = best  
*Light orange italic* = second best.

Backbone	Params	Method	Barbie			Cyberpunk			Expedition			Hornify			Elementfire		
			CLIP $\uparrow$	FID $\downarrow$	Style $\uparrow$	CLIP $\uparrow$	FID $\downarrow$	Style $\uparrow$	CLIP $\uparrow$	FID $\downarrow$	Style $\uparrow$	CLIP $\uparrow$	FID $\downarrow$	Style $\uparrow$	CLIP $\uparrow$	FID $\downarrow$	Style $\uparrow$
SD 2.0	5M	LoRA	<b>35.67</b>	213.42	8.46	33.23	178.17	8.33	31.85	164.21	8.54	32.31	175.16	8.57	32.18	200.45	8.60
		DoRA	35.61	211.63	8.49	33.26	176.48	8.34	31.86	162.93	8.55	32.33	173.12	8.58	32.20	198.55	8.61
		AdaLoRA	35.61	212.45	8.48	33.26	177.30	<i>8.37</i>	<b>31.86</b>	163.61	8.56	<b>32.34</b>	174.12	8.59	32.12	199.50	8.62
		SaRA	35.53	<i>207.12</i>	<i>8.51</i>	<i>33.28</i>	<i>170.81</i>	8.36	31.88	<i>160.37</i>	<i>8.58</i>	32.26	<i>170.28</i>	<i>8.60</i>	<b>32.36</b>	<b>190.28</b>	<i>8.64</i>
		<b>FeRA (Ours)</b>	<b>35.63</b>	<b>201.94</b>	<b>8.52</b>	<b>33.38</b>	<b>166.54</b>	<b>8.39</b>	<b>31.98</b>	<b>156.36</b>	<b>8.61</b>	<b>32.46</b>	<b>166.02</b>	<b>8.63</b>	<i>32.32</i>	<i>191.94</i>	<b>8.65</b>
SD 2.0	20M	LoRA	<b>35.78</b>	198.95	<i>8.74</i>	33.35	165.17	8.45	31.97	152.17	7.57	32.44	162.91	8.53	32.30	186.24	8.22
		DoRA	35.72	197.12	8.15	33.38	164.31	8.52	31.98	151.52	8.03	32.46	160.95	8.15	32.24	184.46	8.62
		AdaLoRA	35.72	197.49	8.31	33.38	164.18	<i>8.76</i>	31.98	152.12	8.17	<b>32.46</b>	161.88	<i>8.56</i>	32.24	185.52	8.64
		SaRA	35.65	<i>192.36</i>	8.44	<i>33.40</i>	<i>158.48</i>	8.34	<b>32.00</b>	<i>149.13</i>	<i>8.54</i>	32.39	<i>158.24</i>	7.99	<b>32.48</b>	<b>177.09</b>	<i>8.76</i>
		<b>FeRA (Ours)</b>	<b>35.74</b>	<b>187.83</b>	<b>8.82</b>	<b>33.50</b>	<b>154.19</b>	<b>8.78</b>	<b>32.12</b>	<b>145.64</b>	<b>8.55</b>	<b>32.58</b>	<b>154.14</b>	<b>8.89</b>	<i>32.44</i>	<i>178.51</i>	<b>8.87</b>
SD 3.0	50M	LoRA	<b>35.80</b>	200.12	8.16	33.37	166.83	<i>8.73</i>	31.98	151.92	8.27	32.45	162.15	8.19	32.31	185.74	<i>8.44</i>
		DoRA	35.74	198.33	8.00	33.40	165.24	7.83	31.99	150.47	8.67	<b>32.47</b>	160.21	8.16	32.25	183.96	8.06
		AdaLoRA	35.74	199.31	<i>8.95</i>	33.40	165.91	8.18	<i>31.99</i>	151.13	8.35	32.47	161.00	8.14	32.25	184.84	8.41
		SaRA	35.67	<i>193.18</i>	8.47	<i>33.42</i>	<i>160.03</i>	7.92	32.01	<i>148.33</i>	<i>8.71</i>	32.40	<i>157.24</i>	<i>8.55</i>	<b>32.49</b>	<b>176.25</b>	7.86
		<b>FeRA (Ours)</b>	<b>35.76</b>	<b>189.20</b>	<b>8.98</b>	<b>33.52</b>	<b>156.31</b>	<b>8.75</b>	<b>32.31</b>	<b>144.65</b>	<b>8.83</b>	<b>32.59</b>	<b>153.36</b>	<b>9.06</b>	<i>32.45</i>	<i>177.72</i>	<b>8.77</b>
FLUX.1	866M	Full-Tuning	35.70	191.00	8.95	33.45	158.60	8.72	32.25	146.20	8.80	32.52	155.10	9.02	32.38	179.90	8.74
		LoRA	36.05	189.08	8.41	33.67	163.46	8.30	31.61	147.65	8.49	32.21	<i>170.31</i>	8.53	32.19	170.39	8.54
		DoRA	<b>36.09</b>	189.62	8.43	<i>33.72</i>	158.02	8.29	31.60	147.18	8.52	32.22	172.16	8.55	32.20	<b>169.27</b>	8.56
		AdaLoRA	<b>36.08</b>	188.91	8.44	33.72	161.51	<i>8.31</i>	31.61	147.43	8.54	32.22	<b>170.12</b>	8.55	<b>32.22</b>	<b>169.80</b>	8.57
		SaRA	36.00	<i>186.50</i>	<i>8.45</i>	33.71	<i>155.22</i>	8.28	<i>31.64</i>	<i>141.02</i>	<i>8.55</i>	<b>33.15</b>	171.27	<i>8.56</i>	<b>32.25</b>	170.32	<i>8.58</i>
FLUX.1	2085M	LoRA	36.15	176.41	8.55	33.78	152.41	7.81	31.72	137.34	<i>8.59</i>	32.33	<b>158.35</b>	8.27	32.30	158.93	8.36
		DoRA	<b>36.20</b>	176.92	<i>8.77</i>	<i>33.83</i>	147.55	<i>8.02</i>	31.71	136.69	7.86	32.34	160.22	8.30	<b>32.31</b>	157.84	8.26
		AdaLoRA	<i>36.19</i>	176.24	8.76	<i>33.83</i>	150.27	7.90	31.71	137.12	8.52	32.34	<i>158.42</i>	8.57	32.31	158.31	<i>8.67</i>
		SaRA	36.10	<i>173.91</i>	8.23	33.82	<i>144.59</i>	7.79	<i>31.75</i>	<i>131.20</i>	7.64	<b>33.27</b>	159.13	<i>8.61</i>	<b>32.36</b>	<i>154.31</i>	7.79
		<b>FeRA (Ours)</b>	<b>36.20</b>	<b>171.55</b>	<b>8.78</b>	<b>33.92</b>	<b>144.22</b>	<b>8.54</b>	<b>31.78</b>	<b>129.43</b>	<b>8.60</b>	<i>32.46</i>	161.94	<b>8.83</b>	31.90	<b>150.86</b>	<b>8.71</b>
FLUX.1	50M	LoRA	36.18	177.48	<i>8.73</i>	33.80	153.13	<i>7.99</i>	31.73	136.72	8.47	32.35	<i>157.87</i>	7.87	32.32	158.71	8.26
		DoRA	36.23	178.63	8.01	<i>33.85</i>	148.74	7.68	31.72	136.24	<i>8.59</i>	32.36	159.64	<i>8.39</i>	<b>32.33</b>	<b>157.53</b>	7.61
		AdaLoRA	<b>36.22</b>	177.64	8.14	33.85	151.95	7.49	31.72	136.54	8.08	32.36	<b>157.53</b>	7.91	32.33	157.54	<i>8.52</i>
		SaRA	36.13	<i>175.13</i>	8.55	<i>33.42</i>	<i>160.03</i>	7.92	32.01	<i>148.33</i>	<i>8.71</i>	32.40	<i>157.24</i>	<i>8.55</i>	<b>32.38</b>	<b>158.12</b>	8.13
		<b>FeRA (Ours)</b>	<b>36.23</b>	<b>172.59</b>	<b>8.81</b>	<b>33.94</b>	<b>145.42</b>	<b>8.42</b>	<b>31.79</b>	<b>128.73</b>	<b>8.65</b>	<i>32.48</i>	161.12	<b>8.76</b>	31.92	<b>154.95</b>	<b>8.57</b>
FLUX.1	7.8B	Full-Tuning	36.15	174.80	8.78	33.85	147.90	8.39	31.72	130.50	8.62	32.40	162.80	8.72	31.85	156.90	8.54
		LoRA	36.05	175.23	8.55	33.61	146.32	<i>8.34</i>	32.08	132.46	8.19	32.65	143.51	<i>8.66</i>	32.52	159.35	7.82
		DoRA	36.01	173.58	8.51	33.64	144.78	8.28	<i>32.10</i>	131.34	<i>8.63</i>	32.67	141.83	8.14	<b>32.75</b>	157.18	7.77
		AdaLoRA	36.03	172.56	8.52	33.65	143.51	8.15	31.98	132.22	8.38	32.66	140.30	7.95	32.49	155.98	8.01
		<b>FeRA (Ours)</b>	<b>36.05</b>	<b>165.87</b>	<b>8.66</b>	<b>33.76</b>	<b>138.05</b>	<b>8.50</b>	32.02	<b>126.18</b>	<b>8.72</b>	<b>32.81</b>	<b>135.75</b>	<b>8.75</b>	<i>32.68</i>	<b>154.37</b>	<b>8.10</b>
FLUX.1	20M	LoRA	36.15	162.79	8.35	33.74	136.43	<i>8.45</i>	32.20	122.19	<i>8.78</i>	32.78	133.40	<i>8.89</i>	32.65	148.53	8.33
		DoRA	36.12	158.92	<i>8.86</i>	33.77	134.34	8.36	32.21	121.77	8.43	<b>32.85</b>	<i>128.05</i>	8.23	32.68	146.44	<i>8.81</i>
		AdaLoRA	36.12	161.46	8.55	33.77	135.16	8.08	<i>32.23</i>	122.73	8.60	32.83	132.63	8.20	32.68	147.62	8.22
		<b>FeRA (Ours)</b>	<b>36.16</b>	<b>156.15</b>	8.28	<i>33.79</i>	<i>131.42</i>	8.21	<i>32.25</i>	<i>120.34</i>	8.50	32.83	129.13	8.30	<b>32.71</b>	<i>143.29</i>	8.39
		LoRA	35.17	163.76	8.43	33.75	136.85	8.39	32.21	122.23	<i>8.65</i>	32.79	132.93	8.43	32.66	148.40	<i>8.78</i>
FLUX.1	50M	DoRA	36.13	159.02	<i>8.71</i>	33.78	135.61	<i>8.97</i>	32.14	121.15	8.02	<b>32.84</b>	131.00	8.28	32.69	145.39	8.65
		AdaLoRA	36.13	162.62	8.55	33.78	135.93	8.64	<i>32.24</i>	121.77	8.06	<b>32.84</b>	131.48	8.92	32.69	146.67	8.34
		SaRA	<b>36.20</b>	<i>156.91</i>	8.18	<i>33.80</i>	<i>131.28</i>	8.19	<i>32.26</i>	<i>119.71</i>	8.55	<i>32.84</i>	<i>128.65</i>	<i>9.00</i>	<i>32.72</i>	<i>143.74</i>	8.64
		<b>FeRA (Ours)</b>	<b>36.17</b>	<b>154.76</b>	<b>9.15</b>	<b>34.90</b>	<b>129.32</b>	<b>9.11</b>	32.15	<b>117.22</b>	<b>8.85</b>	<b>32.95</b>	<b>125.36</b>	<b>9.16</b>	<i>32.82</i>	<b>143.21</b>	<b>9.03</b>
		Full-Tuning	36.13	165.37	8.71	33.81	137.55	8.55	32.17	125.68	8.77	32.86	135.25	8.80	32.80	153.87	8.82

both metrics across all categories. For instance, it attains the best CLIP-I values on all five subjects and top CLIP-T results in four of them, surpassing other PEFT methods by a clear margin. LoRA and DoRA perform competitively in CLIP-I but yield noticeably lower CLIP-T, suggesting overfitting toward visual features at the expense of text alignment. SaRA, while producing the highest CLIP-T on dog, suffers a sharp drop in CLIP-I, reflecting poor balance between fidelity and semantic accuracy. Overall,

FeRA demonstrates the best trade-off between subject identity preservation and text-image alignment, validating its effectiveness and generalizability in personalized image generation. As illustrated in Fig. 5, FeRA produces clearer textures and more accurate colors across all prompts. It preserves structural coherence and fine details, yielding sharper boundaries, more faithful appearance, and more stable rendering across diverse visual conditions, consistently outperforming existing PEFT baselines in visual quality.



Figure 4. Comparison of the generated images between different PEFT methods.

Table 2. Quantitative comparison between different PEFT methods on image customization. **Red bold** = best, *orange italic* = second best.

Methods	Dog		Clock		Backpack		Toy Duck		Teapot	
	CLIP-I ↑	CLIP-T ↑								
Dreambooth + Full-tuning	0.788	24.15	0.789	23.15	0.654	24.09	0.790	24.05	0.750	24.12
Dreambooth + LoRA	<i>0.895</i>	23.64	0.913	21.71	<i>0.917</i>	25.23	0.905	23.80	0.906	23.58
Dreambooth + DoRA	0.897	23.71	<i>0.915</i>	21.78	0.914	<i>25.31</i>	<i>0.907</i>	23.88	<i>0.908</i>	23.65
Dreambooth + AdaLoRA	0.896	23.69	0.914	21.76	0.917	25.29	0.906	23.85	0.907	23.63
Dreambooth + SaRA	0.790	<b>25.97</b>	0.887	<i>23.51</i>	0.886	25.27	0.885	<b>25.50</b>	0.866	<i>25.12</i>
<b>Dreambooth + FeRA (Ours)</b>	<b>0.900</b>	<i>25.95</i>	<b>0.920</b>	<b>23.63</b>	<b>0.925</b>	<b>25.35</b>	<b>0.910</b>	<i>24.60</i>	<b>0.913</b>	<b>25.32</b>



Figure 5. DreamBooth results across PEFT methods. FeRA delivers more consistent identity and cleaner compositions.

### 5.3. Ablation Studies

To comprehensively examine the individual contribution and practical influence of each component in FeRA, we conduct detailed ablation studies on the Frequency-Energy Indicator (FEI), the soft frequency router, the Frequency-

Energy Consistency Loss (FECL), the predefined number of frequency bands, and the total number of LoRA experts. All experiments are systematically performed on Stable Diffusion 2.0 using the Cyberpunk dataset under identical training budgets to ensure a controlled and fair compar-

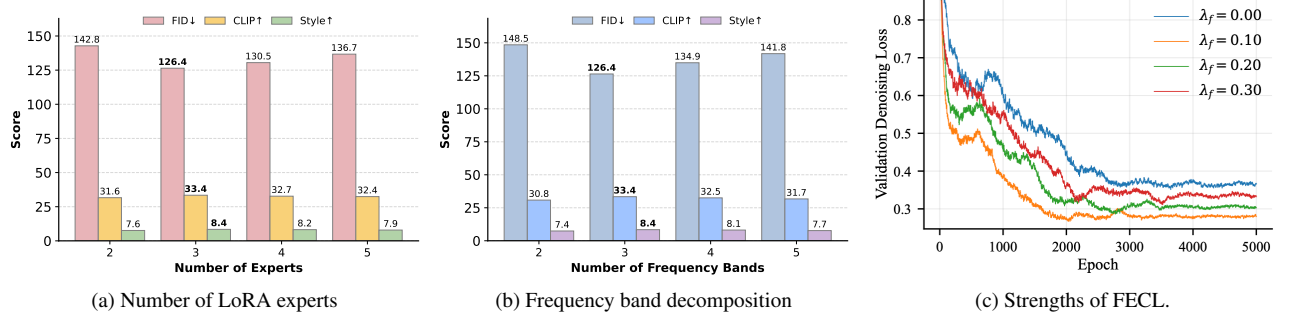


Figure 6. Ablation on design factors of FeRA: (a) LoRA expert number, (b) frequency decomposition, and (c) the strengths of FECL.

Table 3. Ablation on routing configurations. “FEI” denotes the proposed frequency–energy indicator, and “Soft Router” refers to the soft routing mechanism. Removing FEI falls back to timestep-based routing. “✓” and “✗” indicate whether each module is enabled.

FEI	Soft Router	CLIP↑	FID↓	Style↑
✗	✗	30.12	138.50	7.42
✓	✗	31.84	132.70	7.93
✗	✓	31.10	134.90	7.68
✓	✓	<b>32.96</b>	<b>126.40</b>	<b>8.21</b>

ison across variants.

**Frequency-Energy Indicator and Soft Router.** Tab. 3 reports that replacing timestep-based routing with FEI improves FID, CLIP, and Style scores, indicating that frequency composition offers a more informative signal than discrete step indices. Soft routing alone yields a small gain, while combining it with FEI stabilizes expert selection and achieves the best overall balance across metrics.

**The number of Experts.** Under the three-band setting, Figure 6 (a) compares different numbers of LoRA experts. Using one expert per band (*i.e.*, three in total) achieves the best performance across FID, CLIP, and Style metrics. This confirms that frequency-specialized experts enable more efficient and interpretable adaptation.

**The number of Frequency Band.** We vary the number of frequency bands used for spectral decomposition in FEI. As shown in Figure 6 (b), three bands (*i.e.*, low, mid, high) consistently outperform two or more than three. This indicates that a three-band division captures semantic structure while avoiding redundancy and over-fragmentation.

**Frequency-Energy Consistency Loss.** Figure 6 (c) shows the impact of different FECL weights  $\lambda_f \in \{0, 0.1, 0.2, 0.3\}$ . A small weight accelerates and stabilizes convergence, whereas removing FECL slows optimization and larger weights cause oscillation. Moderate regularization achieves the best trade-off between stability and generalization.

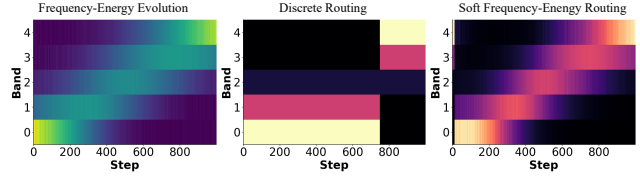


Figure 7. Compared with discrete routing strategy.

#### 5.4. Our Soft Frequency-Eneny Routing Analysis

A representative discrete routing strategy employs a expert MoE design for diffusion denoising: a high-noise expert for early steps that captures global structure, and a low-noise expert for later steps that refines details. The routing is typically governed by a monotonic SNR schedule with a single threshold, resulting in a hard switch between experts. Such a scheme is adopted, for example, in Wan2.2 [49]. Although this threshold-based routing can be extended to multi-LoRA settings for comparison, it inherently enforces a discrete expert transition. To visualize the behavioral difference, we plot the Frequency-Energy Evolution and the corresponding routing weights as heatmaps (Fig. 7). The discrete routing shows an abrupt switch between low- and high-frequency bands, whereas our frequency-aware routing produces a smooth transition that follows the spectral energy migration. This continuity enables finer control and better alignment between the model’s update behavior and the evolving frequency composition during denoising.

## 6. Conclusion

We propose FeRA, a parameter-efficient fine-tuning framework for diffusion models guided by the frequency-energy state of latent representations. It comprises three lightweight modules: a Frequency-Energy Indicator for bandwise energy analysis, a Soft Router for frequency-specific expert blending, and a Frequency-Energy Consistency Loss for stable optimization. By aligning adaptation with the frequency-energy in the denoising process, FeRA adds minimal overhead and integrates seamlessly into existing diffusion backbones. This design explicitly exploits the

natural frequency-energy hierarchy in diffusion trajectories, allowing the model to focus adaptation on the most informative frequency bands. Extensive experiments show consistent gains in fidelity, alignment, and style, clearly demonstrating that frequency-energy awareness provides an effective and interpretable route to diffusion adaptation.

## References

- [1] Jatin Kumar Arora, Sudhar Rajagopalan, Jaskaran Singh, and Ashish Purohit. Low-frequency adaptation-deep neural network-based domain adaptation approach for shaft imbalance fault diagnosis. *Journal of Vibration Engineering & Technologies*, 12(1):375–394, 2024. [3](#)
- [2] Jinze Bai, Shuai Bai, Yunfei Chu, Zeyu Cui, Kai Dang, Xiaodong Deng, Yang Fan, Wenbin Ge, Yu Han, Fei Huang, et al. Qwen technical report. *arXiv preprint arXiv:2309.16609*, 2023. [5](#)
- [3] Yoshua Bengio, Aaron Courville, and Pascal Vincent. Representation learning: A review and new perspectives. *IEEE transactions on pattern analysis and machine intelligence*, 35(8):1798–1828, 2013. [3](#)
- [4] Andreas Blattmann, Tim Dockhorn, Sumith Kulal, Daniel Mendelevitch, Maciej Kilian, Dominik Lorenz, Yam Levi, Zion English, Vikram Voleti, Adam Letts, et al. Stable video diffusion: Scaling latent video diffusion models to large datasets. *arXiv preprint arXiv:2311.15127*, 2023. [2](#)
- [5] Shilei Cao, Hehai Lin, Jiashun Cheng, Yang Liu, Guowen Li, Xuehe Wang, Juepeng Zheng, Haoyuan Liang, Meng Jin, Chengwei Qin, et al. Task-adaptive parameter-efficient fine-tuning for weather foundation models. *arXiv preprint arXiv:2509.22020*, 2025. [2](#)
- [6] Changgu Chen, Libing Yang, Xiaoyan Yang, Lianggangxu Chen, Gaoqi He, Changbo Wang, and Yang Li. Find: Fine-tuning initial noise distribution with policy optimization for diffusion models. In *Proceedings of the 32nd ACM International Conference on Multimedia*, pages 6735–6744, 2024. [2](#)
- [7] William Fedus, Barret Zoph, and Noam Shazeer. Switch transformers: Scaling to trillion parameter models with simple and efficient sparsity. *Journal of Machine Learning Research*, 23(120):1–39, 2022. [3](#)
- [8] David J Field. Relations between the statistics of natural images and the response properties of cortical cells. *Journal of the Optical Society of America A*, 4(12):2379–2394, 1987. [3](#)
- [9] Rinon Gal, Yuval Alaluf, Yuval Atzmon, Or Patashnik, Amit H Bermano, Gal Chechik, and Daniel Cohen-Or. An image is worth one word: Personalizing text-to-image generation using textual inversion. *arXiv preprint arXiv:2208.01618*, 2022. [1, 2](#)
- [10] Alireza Ganjdanesh, Yan Kang, Yuchen Liu, Richard Zhang, Zhe Lin, and Heng Huang. Mixture of efficient diffusion experts through automatic interval and sub-network selection. In *European Conference on Computer Vision*, pages 54–71. Springer, 2024. [3](#)
- [11] Demi Guo, Alexander M Rush, and Yoon Kim. Parameter-efficient transfer learning with diff pruning. *arXiv preprint arXiv:2012.07463*, 2020. [2](#)
- [12] Yuwei Guo, Ceyuan Yang, Anyi Rao, Zhengyang Liang, Yaohui Wang, Yu Qiao, Maneesh Agrawala, Dahua Lin, and Bo Dai. Animatediff: Animate your personalized text-to-image diffusion models without specific tuning. *arXiv preprint arXiv:2307.04725*, 2023. [2](#)
- [13] Jonathan Ho, Ajay Jain, and Pieter Abbeel. Denoising diffusion probabilistic models. *Advances in neural information processing systems*, 33:6840–6851, 2020. [1, 2, 3](#)
- [14] Neil Houlsby, Andrei Giurgiu, Stanislaw Jastrzebski, Bruna Morrone, Quentin De Laroussilhe, Andrea Gesmundo, Mona Attariyan, and Sylvain Gelly. Parameter-efficient transfer learning for nlp. In *International conference on machine learning*, pages 2790–2799. PMLR, 2019. [1](#)
- [15] Edward J Hu, Yelong Shen, Phillip Wallis, Zeyuan Allen-Zhu, Yuanzhi Li, Shean Wang, Lu Wang, Weizhu Chen, et al. Lora: Low-rank adaptation of large language models. *ICLR*, 1(2):3, 2022. [1, 2, 5](#)
- [16] Teng Hu, Jiangning Zhang, Ran Yi, Hongrui Huang, Yabiao Wang, and Lizhuang Ma. High-efficient diffusion model fine-tuning with progressive sparse low-rank adaptation. In *13th International Conference on Learning Representations, ICLR 2025*, pages 92066–92078. International Conference on Learning Representations, ICLR, 2025. [3, 5](#)
- [17] Xiaobin Hu, Wenqi Ren, John LaMaster, Xiaochun Cao, Xiaoming Li, Zechao Li, Bjoern Menze, and Wei Liu. Face super-resolution guided by 3d facial priors. In *European Conference on Computer Vision*, pages 763–780. Springer, 2020. [1](#)
- [18] Xiaozhong Ji, Chuming Lin, Zhonggan Ding, Ying Tai, Junwei Zhu, Xiaobin Hu, Donghao Luo, Yanhao Ge, and Chengjie Wang. Realtalk: Real-time and realistic audio-driven face generation with 3d facial prior-guided identity alignment network. *arXiv preprint arXiv:2406.18284*, 2024. [1](#)
- [19] Xiaozhong Ji, Xiaobin Hu, Zhihong Xu, Junwei Zhu, Chuming Lin, Qingdong He, Jiangning Zhang, Donghao Luo, Yi Chen, Qin Lin, et al. Sonic: Shifting focus to global audio perception in portrait animation. In *Proceedings of the Computer Vision and Pattern Recognition Conference*, pages 193–203, 2025. [1](#)
- [20] Tero Karras, Miika Aittala, Timo Aila, and Samuli Laine. Elucidating the design space of diffusion-based generative models. *Advances in neural information processing systems*, 35:26565–26577, 2022. [2](#)
- [21] Diederik P Kingma, Max Welling, et al. An introduction to variational autoencoders. *Foundations and Trends® in Machine Learning*, 12(4):307–392, 2019. [3](#)
- [22] Huibert Kwakernaak and Raphael Sivan. Modern signals and systems. *NASA STI/Recon Technical Report A*, 91:11586, 1991. [4](#)
- [23] Kaiyang Li, Shaobo Han, Qing Su, Wei Li, Zhipeng Cai, and Shihao Ji. Uni-lora: One vector is all you need. *arXiv preprint arXiv:2506.00799*, 2025. [3](#)

[24] Yunxiang Li, Hua-Chieh Shao, Xiao Liang, Liyuan Chen, Ruiqi Li, Steve Jiang, Jing Wang, and You Zhang. Zero-shot medical image translation via frequency-guided diffusion models. *IEEE transactions on medical imaging*, 43(3):980–993, 2023. 2

[25] Shih-Yang Liu, Chien-Yi Wang, Hongxu Yin, Pavlo Molchanov, Yu-Chiang Frank Wang, Kwang-Ting Cheng, and Min-Hung Chen. Dora: Weight-decomposed low-rank adaptation. In *Forty-first International Conference on Machine Learning*, 2024. 5

[26] Tianlin Liu, Mathieu Blondel, Carlos Riquelme, and Joan Puigcerver. Routers in vision mixture of experts: An empirical study. *arXiv preprint arXiv:2401.15969*, 2024. 3

[27] Xiao Liu, Kaixuan Ji, Yicheng Fu, Weng Tam, Zhengxiao Du, Zhilin Yang, and Jie Tang. P-tuning: Prompt tuning can be comparable to fine-tuning across scales and tasks. In *Proceedings of the 60th Annual Meeting of the Association for Computational Linguistics (Volume 2: Short Papers)*, pages 61–68, 2022. 2

[28] David G Lowe. Distinctive image features from scale-invariant keypoints. *International journal of computer vision*, 60(2):91–110, 2004. 3

[29] Chong Mou, Xiantao Wang, Liangbin Xie, Yanze Wu, Jian Zhang, Zhongang Qi, and Ying Shan. T2i-adapter: Learning adapters to dig out more controllable ability for text-to-image diffusion models. In *Proceedings of the AAAI conference on artificial intelligence*, pages 4296–4304, 2024. 1, 2, 3

[30] Alexander Quinn Nichol and Prafulla Dhariwal. Improved denoising diffusion probabilistic models. In *International conference on machine learning*, pages 8162–8171. PMLR, 2021. 2

[31] Ben Poole, Ajay Jain, Jonathan T Barron, and Ben Mildenhall. Dreamfusion: Text-to-3d using 2d diffusion. *arXiv preprint arXiv:2209.14988*, 2022. 1, 2

[32] Vadim Popov, Ivan Vovk, Vladimir Gogoryan, Tasnima Sadekova, and Mikhail Kudinov. Grad-tts: A diffusion probabilistic model for text-to-speech. In *International conference on machine learning*, pages 8599–8608. PMLR, 2021. 2

[33] Alec Radford, Jong Wook Kim, Chris Hallacy, Aditya Ramesh, Gabriel Goh, Sandhini Agarwal, Girish Sastry, Amanda Askell, Pamela Mishkin, Jack Clark, et al. Learning transferable visual models from natural language supervision. In *International conference on machine learning*, pages 8748–8763. PMLR, 2021. 1

[34] Aditya Ramesh, Prafulla Dhariwal, Alex Nichol, Casey Chu, and Mark Chen. Hierarchical text-conditional image generation with clip latents. *arXiv preprint arXiv:2204.06125*, 1(2):3, 2022. 5

[35] Carlos Riquelme, Joan Puigcerver, Basil Mustafa, Maxim Neumann, Rodolphe Jenatton, André Susano Pinto, Daniel Keysers, and Neil Houlsby. Scaling vision with sparse mixture of experts. *Advances in Neural Information Processing Systems*, 34:8583–8595, 2021. 3

[36] Robin Rombach, Andreas Blattmann, Dominik Lorenz, Patrick Esser, and Björn Ommer. High-resolution image synthesis with latent diffusion models. In *Proceedings of the IEEE/CVF conference on computer vision and pattern recognition*, pages 10684–10695, 2022. 1, 2, 3

[37] Daniel Ruderman and William Bialek. Statistics of natural images: Scaling in the woods. *Advances in neural information processing systems*, 6, 1993. 3

[38] Nataniel Ruiz, Yuanzhen Li, Varun Jampani, Yael Pritch, Michael Rubinstein, and Kfir Aberman. Dreambooth: Fine tuning text-to-image diffusion models for subject-driven generation. In *Proceedings of the IEEE/CVF conference on computer vision and pattern recognition*, pages 22500–22510, 2023. 1, 2, 5

[39] Tim Salimans and Jonathan Ho. Progressive distillation for fast sampling of diffusion models. *arXiv preprint arXiv:2202.00512*, 2022. 1

[40] Robin San-Roman, Eliya Nachmani, and Lior Wolf. Noise estimation for generative diffusion models. *arXiv preprint arXiv:2104.02600*, 2021. 2

[41] Noam Shazeer, Azalia Mirhoseini, Krzysztof Maziarz, Andy Davis, Quoc Le, Geoffrey Hinton, and Jeff Dean. Outrageously large neural networks: The sparsely-gated mixture-of-experts layer. *arXiv preprint arXiv:1701.06538*, 2017. 3

[42] Uriel Singer, Adam Polyak, Thomas Hayes, Xi Yin, Jie An, Songyang Zhang, Qiyuan Hu, Harry Yang, Oron Ashual, Oran Gafni, et al. Make-a-video: Text-to-video generation without text-video data. *arXiv preprint arXiv:2209.14792*, 2022. 2

[43] Yang Song, Jascha Sohl-Dickstein, Diederik P Kingma, Abhishek Kumar, Stefano Ermon, and Ben Poole. Score-based generative modeling through stochastic differential equations. *arXiv preprint arXiv:2011.13456*, 2020. 2

[44] Yang Song, Prafulla Dhariwal, Mark Chen, and Ilya Sutskever. Consistency models. 2023. 1, 2

[45] Yiren Song, Cheng Liu, and Mike Zheng Shou. Makeanything: Harnessing diffusion transformers for multi-domain procedural sequence generation. *arXiv preprint arXiv:2502.01572*, 2025. 2

[46] Yiren Song, Cheng Liu, and Mike Zheng Shou. Omniconsistency: Learning style-agnostic consistency from paired stylization data. *arXiv preprint arXiv:2505.18445*, 2025. 2

[47] Matthew Tivnan, Jacopo Teneggi, Tzu-Cheng Lee, Ruqiao Zhang, Kirsten Boedeker, Liang Cai, Grace J Gang, Jeremias Sulam, and J Webster Stayman. Fourier diffusion models: A method to control mtf and nps in score-based stochastic image generation. *IEEE transactions on medical imaging*, 2025. 3

[48] Asaf Valadarsky, Michael Schapira, Dafna Shahaf, and Aviv Tamar. Learning to route. In *Proceedings of the 16th ACM workshop on hot topics in networks*, pages 185–191, 2017. 3

[49] Team Wan, Ang Wang, Baole Ai, Bin Wen, Chaojie Mao, Chen-Wei Xie, Di Chen, Fei Yu, Haiming Zhao, Jianxiao Yang, et al. Wan: Open and advanced large-scale video generative models. *arXiv preprint arXiv:2503.20314*, 2025. 8

[50] Haochen Wang, Xiaodan Du, Jiahao Li, Raymond A Yeh, and Greg Shakhnarovich. Score jacobian chaining: Lifting pretrained 2d diffusion models for 3d generation. In *Proceedings of the IEEE/CVF conference on computer vision and pattern recognition*, pages 12619–12629, 2023. 2

- [51] Hu Xiaobin, Liang Yujie, Luo Donghao, Peng Xu, Zhang Jiangning, Zhu Junwei, Wang Chengjie, and Fu Yanwei. Vt-bench: Comprehensive benchmark suite towards real-world virtual try-on models. *arXiv preprint arXiv:2505.19571*, 2025. 1
- [52] Kai Xu, Minghai Qin, Fei Sun, Yuhao Wang, Yen-Kuang Chen, and Fengbo Ren. Learning in the frequency domain. In *Proceedings of the IEEE/CVF conference on computer vision and pattern recognition*, pages 1740–1749, 2020. 3
- [53] Hu Ye, Jun Zhang, Sibo Liu, Xiao Han, and Wei Yang. Ip-adapter: Text compatible image prompt adapter for text-to-image diffusion models. *arXiv preprint arXiv:2308.06721*, 2023. 2, 3
- [54] Bo Yin, Xingyi Yang, and Xinchao Wang. Don’t forget the nonlinearity: Unlocking activation functions in efficient fine-tuning. *arXiv preprint arXiv:2509.13240*, 2025. 3
- [55] Cuihong Yu, Cheng Han, and Chao Zhang. Dmfft: improving the generation quality of diffusion models using fast fourier transform. *Scientific Reports*, 15(1):10200, 2025. 3
- [56] Lvmin Zhang, Anyi Rao, and Maneesh Agrawala. Adding conditional control to text-to-image diffusion models. In *Proceedings of the IEEE/CVF international conference on computer vision*, pages 3836–3847, 2023. 1, 2, 3
- [57] Qingru Zhang, Minshuo Chen, Alexander Bukharin, Nikos Karampatziakis, Pengcheng He, Yu Cheng, Weizhu Chen, and Tuo Zhao. Adalora: Adaptive budget allocation for parameter-efficient fine-tuning. *arXiv preprint arXiv:2303.10512*, 2023. 3, 5
- [58] Pengfei Zhu, Yang Sun, Bing Cao, and Qinghua Hu. Task-customized mixture of adapters for general image fusion. In *Proceedings of the IEEE/CVF conference on computer vision and pattern recognition*, pages 7099–7108, 2024. 3



# FeRA: Frequency-Energy Constrained Routing for Effective Diffusion Adaptation Fine-Tuning

## Supplementary Material

### 7. MLLM-Judge Prompt

In experiment we evaluate stylistic fidelity(Style Score) using an MLLM-based style assessor. The model is prompted to judge the stylistic attributes of the generated images. For transparency and reproducibility, we include the exact prompt used in all evaluations below.

```
You are a strict T2I style judge.  
Evaluate ONLY the STYLE qualities of the output image.  
Use style cues from the PROMPT (and optional STYLE_TEXT / STYLE refs).  
Ignore all semantic correctness.  
  
Return a compact JSON with:  
style_faithfulness, style_intensity,  
palette_match, lighting_mood,  
texture_pattern, artifacts,  
overall_style.  
Each score is in [0,10] (integer or one decimal). No extra text.  
  
Definitions:  
- style_faithfulness: reflection of style cues (medium, era, motifs).  
- style_intensity: stylization strength (not too weak or excessive).  
- palette_match: color palette and tone mapping.  
- lighting_mood: lighting style and ambience.  
- texture_pattern: local texture/strokes/pattern effects.  
- artifacts: fewer visual artifacts  $\Rightarrow$  higher score.  
- overall_style = 0.30*style_faithfulness  
+ 0.15*style_intensity  
+ 0.20*palette_match + 0.15*lighting_mood  
+ 0.20*texture_pattern.
```

### 8. Experiment Setting

For clarity and reproducibility, we summarize the common training configuration used across all experiments in Table 4.

### 9. Other Experiment Result

#### 9.1. Text-to-Image Style Adaptation

To further examine the generality of our training pipeline, we extend the text-to-image style adaptation experiments to multiple diffusion backbones with distinct latent resolutions, denoising trajectories, and text-image alignment capabilities. This broader evaluation helps disentangle whether the observed performance gains truly stem from our frequency-energy-guided fine-tuning strategy rather than from accidental synergy with a particular pretrained model. By comparing models that differ substantially in their architectural design and training dynamics, we can more reliably assess the stability and scalability of our method.

As summarized in Tab. 5, the performance trends remain consistent across Stable Diffusion 1.5 and Stable Diffusion XL. Despite the large gap in model capacity and latent-space structure, our approach produces clear improvements in perceptual quality, stylistic faithfulness, and controllability. At the same time, semantic alignment remains competitive, suggesting that the additional style expressiveness does not come at the cost of prompt consistency. These results indicate that our fine-tuning strategy transfers reliably across diffusion families and retains its benefits even as the backbone scale or architecture changes.

And we also show others qualitative result in other datasets or backbones in Fig. 8, 9 and 10.

#### 9.2. Image Customization

We further study instance-level image customization under DreamBooth fine-tuning on two backbones, Stable Diffusion 1.5 and Stable Diffusion 3.0. This setting evaluates how well different PEFT approaches preserve the identity of a specific object while retaining prompt alignment. Tab. 6 and 7 report CLIP-based image alignment (CLIP-I) and text alignment (CLIP-T).

Across both backbones, FeRA consistently achieves the best or second-best instance faithfulness (CLIP-I) while maintaining competitive or superior text alignment (CLIP-T) compared to LoRA, DoRA, AdaLoRA and SaRA. The trend is stable on both the lighter SD 1.5 and the stronger SD 3.0 models, indicating that our framework provides robust benefits for DreamBooth-style image customization across different backbone capacities.

And we also show others qualitative result in other datasets in Fig. 11.

Table 4. Common experiment settings used throughout our study.

Category	Setting
Base Model	frozen VAE and text encoder
LoRA Config	applied to attention modules ( <code>to_q</code> , <code>to_k</code> , <code>to_v</code> , <code>to_out</code> )
Resolution	$512 \times 512$ (resize + center/random crop)
Batch Size	16 per device
Training Steps	5000
Optimizer	AdamW, $LR = 1 \times 10^{-4}$ , weight decay = 0.01
Warmup Steps	500
Scheduler	DDPM scheduler with standard noise schedule
Mixed Precision	fp16
Grad Norm Clip	1.0
Inference	30-step DDPM sampling
Hardware	NVIDIA H100 GPUs

Table 5. Comparison with different parameter-efficient fine-tuning methods on Stable Diffusion 1.5 and SDXL. **Orange bold** = best *Light orange italic* = second best.

Backbone	Params	Method	Barbie			Cyberpunk			Expedition			Hornify			Elementfire		
			CLIP ↑	FID ↓	Style ↑	CLIP ↑	FID ↓	Style ↑	CLIP ↑	FID ↓	Style ↑	CLIP ↑	FID ↓	Style ↑	CLIP ↑	FID ↓	Style ↑
SD 1.5	5M	LoRA	<b>35.19</b>	194.73	8.37	33.16	<i>129.63</i>	8.14	31.51	128.73	8.46	31.08	163.02	8.48	<b>31.59</b>	<i>156.95</i>	8.47
		DoRA	35.12	193.90	8.36	<b>33.20</b>	131.51	<i>8.19</i>	31.53	129.13	8.47	31.15	164.24	8.50	<b>31.62</b>	158.59	8.49
		AdaLoRA	<b>35.12</b>	194.30	8.38	33.12	131.51	8.17	31.53	129.00	<b>8.50</b>	31.15	<i>162.81</i>	8.49	31.55	<b>156.62</b>	8.51
		SaRA	35.01	<i>190.81</i>	<i>8.39</i>	<b>33.18</b>	138.01	8.18	<b>31.56</b>	<i>128.50</i>	8.49	<b>31.18</b>	163.50	<i>8.51</i>	31.55	166.00	<i>8.52</i>
		<b>FeRA (Ours)</b>	34.34	<b>184.98</b>	<b>8.43</b>	32.96	<b>126.40</b>	<b>8.21</b>	<b>31.66</b>	<b>127.03</b>	<b>8.53</b>	<b>31.20</b>	<b>162.28</b>	<b>8.54</b>	31.12	164.92	<b>8.55</b>
	20M	LoRA	<b>35.31</b>	181.15	8.58	33.25	122.32	<i>8.04</i>	31.60	120.10	8.05	31.19	151.75	7.94	<b>31.70</b>	<i>146.50</i>	7.72
		DoRA	35.25	180.32	8.01	33.22	122.32	7.59	31.63	120.12	<i>8.13</i>	31.25	152.12	<i>8.34</i>	31.64	155.32	<i>8.27</i>
		AdaLoRA	<b>35.25</b>	180.70	<i>8.60</i>	<b>33.22</b>	<i>122.30</i>	7.83	31.63	119.95	7.58	31.25	<i>151.45</i>	8.31	31.62	<b>146.11</b>	8.17
		SaRA	35.15	<i>177.50</i>	8.06	<b>33.28</b>	127.80	7.70	<b>31.67</b>	<i>119.50</i>	7.96	<b>31.29</b>	152.18	7.90	<i>31.66</i>	155.09	7.61
		<b>FeRA (Ours)</b>	34.50	<b>172.03</b>	<b>8.74</b>	<b>33.38</b>	<b>117.90</b>	<b>8.32</b>	<b>31.78</b>	<b>118.11</b>	<b>8.55</b>	<b>31.32</b>	<b>150.91</b>	<b>8.71</b>	31.25	153.62	<b>8.60</b>
	50M	LoRA	<b>35.35</b>	183.42	8.26	<b>33.28</b>	123.55	7.58	31.62	119.21	8.22	31.22	150.89	<i>8.62</i>	<b>31.73</b>	<i>145.58</i>	8.09
		DoRA	<b>35.29</b>	182.63	<i>8.63</i>	33.25	123.52	7.43	31.65	119.22	8.44	31.28	151.63	7.69	<i>31.69</i>	154.72	<i>8.21</i>
		AdaLoRA	35.29	182.92	8.16	33.25	<i>123.35</i>	<i>8.19</i>	31.65	119.05	<b>8.52</b>	31.28	<i>150.47</i>	8.24	31.69	<b>145.54</b>	7.83
		SaRA	35.19	<i>179.72</i>	8.27	<b>33.31</b>	129.14	7.59	<i>31.69</i>	<i>118.61</i>	<i>8.53</i>	<b>31.32</b>	151.83	8.21	31.49	154.32	7.57
		<b>FeRA (Ours)</b>	34.55	<b>174.21</b>	<b>8.76</b>	33.12	<b>119.13</b>	<b>8.34</b>	<b>31.80</b>	<b>117.21</b>	<b>8.62</b>	<b>31.35</b>	<b>150.13</b>	<b>8.66</b>	31.29	152.48	<b>8.54</b>
	860M	Full-Tuning	34.48	176.50	8.70	33.05	121.20	8.30	31.75	119.00	8.58	31.30	151.80	8.63	31.20	154.00	8.51
SDXL	5M	LoRA	<b>35.88</b>	188.41	8.53	33.45	157.92	8.38	31.94	141.52	8.60	32.45	155.82	8.66	32.32	173.73	8.67
		DoRA	35.83	186.78	8.52	33.48	156.21	8.41	31.96	140.28	8.63	32.48	153.94	8.65	32.35	171.35	8.68
		AdaLoRA	35.85	187.60	<i>8.55</i>	33.49	157.12	8.40	31.97	140.92	8.62	32.48	154.90	8.66	32.32	172.55	<i>8.70</i>
		SaRA	35.76	<b>183.25</b>	8.54	<b>33.51</b>	<b>152.69</b>	<b>8.43</b>	<b>31.98</b>	<b>138.15</b>	<b>8.64</b>	<b>32.51</b>	<b>151.07</b>	<b>8.67</b>	<b>32.38</b>	<b>168.22</b>	8.69
		<b>FeRA (Ours)</b>	<b>35.86</b>	<b>178.67</b>	<b>8.57</b>	<b>33.61</b>	<b>148.88</b>	<b>8.44</b>	<b>32.08</b>	<b>134.69</b>	<b>8.67</b>	<b>32.49</b>	<b>147.29</b>	<b>8.70</b>	<b>32.48</b>	<b>163.51</b>	<b>8.72</b>
	20M	LoRA	<b>35.99</b>	175.23	8.36	33.57	146.84	8.74	32.07	131.42	8.44	32.58	144.90	8.28	32.45	161.42	8.05
		DoRA	35.94	173.73	8.87	33.60	145.72	7.97	32.09	130.17	7.88	32.61	143.12	<i>8.53</i>	32.45	159.15	<i>8.93</i>
		AdaLoRA	35.94	174.25	8.46	33.60	146.45	<i>8.77</i>	32.09	130.82	<i>8.55</i>	32.61	144.00	8.66	32.45	160.22	8.64
		SaRA	35.87	<i>170.44</i>	<i>8.88</i>	<b>33.63</b>	<i>141.93</i>	7.91	<b>32.11</b>	<b>128.26</b>	8.22	<b>32.64</b>	<i>140.23</i>	8.30	<i>32.51</i>	<i>156.25</i>	8.27
		<b>FeRA (Ours)</b>	<b>35.97</b>	<b>166.61</b>	<b>8.94</b>	<b>33.73</b>	<b>138.45</b>	<b>8.82</b>	<b>32.21</b>	<b>128.29</b>	<b>8.68</b>	<b>32.62</b>	<b>136.38</b>	<b>8.92</b>	<b>32.61</b>	<b>152.11</b>	<b>8.95</b>
	50M	LoRA	<b>36.01</b>	176.41	<i>9.09</i>	33.59	147.19	8.45	32.08	130.18	8.23	32.59	144.24	<i>9.11</i>	32.46	160.58	8.23
	3.5B	DoRA	35.96	174.96	8.42	33.62	146.13	8.24	32.10	129.54	8.03	32.62	142.48	9.05	32.46	158.52	8.49
		AdaLoRA	35.96	175.57	8.63	33.62	147.51	<i>8.82</i>	32.10	130.22	8.80	32.62	143.35	9.03	32.46	159.26	<i>8.85</i>
		SaRA	35.89	<i>171.66</i>	8.89	<b>33.65</b>	<b>143.52</b>	8.57	<b>32.12</b>	<b>127.66</b>	<b>8.24</b>	<b>32.65</b>	<i>139.61</i>	8.98	<i>32.52</i>	<i>155.56</i>	8.72
		<b>FeRA (Ours)</b>	<b>35.99</b>	<b>167.33</b>	<b>9.12</b>	<b>33.75</b>	<b>139.51</b>	<b>9.05</b>	<b>32.22</b>	<b>124.21</b>	<b>8.99</b>	<b>32.63</b>	<b>136.11</b>	<b>9.23</b>	<b>32.62</b>	<b>151.46</b>	<b>8.86</b>
		Full-Tuning	36.00	170.80	9.10	33.72	143.00	8.80	32.15	126.50	8.90	32.65	139.00	9.00	32.55	153.00	8.85

### 9.3. Inference-Time Comparison

To assess computational overhead, we report a theoretical runtime comparison between LoRA and our FeRA framework across different backbones (Table 8). All models share

identical sampling steps, ensuring a fair comparison. FeRA introduces lightweight routing and frequency-aware operations, which add only a modest overhead of 8–20%. The results show that FeRA remains close to the efficiency of standard LoRA while providing significantly improved genera-

Table 6. Quantitative comparison between different PEFT methods on image customization (Stable Diffusion 1.5). **Red bold** = best, **orange italic** = second best.

Methods	Dog		Clock		Backpack		Toy Duck		Teapot	
	CLIP-I ↑	CLIP-T ↑								
Dreambooth + Full-tuning	0.788	24.15	0.789	23.15	0.654	24.09	0.790	24.05	0.750	24.12
Dreambooth + LoRA	<b>0.895</b>	23.64	0.913	21.71	<b>0.917</b>	25.23	0.905	23.80	0.906	23.58
Dreambooth + DoRA	<b>0.897</b>	23.71	<b>0.915</b>	21.78	<b>0.914</b>	<b>25.31</b>	<b>0.907</b>	23.88	<b>0.908</b>	23.65
Dreambooth + AdaLoRA	0.896	23.69	0.914	21.76	0.917	25.29	0.906	23.85	0.907	23.63
Dreambooth + SaRA	0.790	<b>25.97</b>	0.887	<b>23.51</b>	0.886	25.27	0.885	<b>25.50</b>	0.866	<b>25.12</b>
<b>Dreambooth + FeRA (Ours)</b>	<b>0.900</b>	<b>25.95</b>	<b>0.920</b>	<b>23.63</b>	<b>0.925</b>	<b>25.35</b>	<b>0.910</b>	<b>24.60</b>	<b>0.913</b>	<b>25.32</b>



Figure 8. Comparison of the generated images between different PEFT methods in other datasets.



Figure 9. Comparison of the generated images between different PEFT methods(SD1.5).

tion quality and controllability.



Figure 10. Comparison of the generated images between different PEFT methods(SD3.0).



Figure 11. Comparison of the image customization between different PEFT methods.

Table 7. Quantitative comparison between different PEFT methods on image customization (Stable Diffusion 3.0). **Red bold** = best, **orange italic** = second best.

Methods	Dog		Clock		Backpack		Toy Duck		Teapot	
	CLIP-I ↑	CLIP-T ↑								
Dreambooth + Full-tuning	0.798	24.55	0.799	23.55	0.664	24.49	0.800	24.45	0.760	24.52
Dreambooth + LoRA	0.905	24.04	0.923	22.11	<i>0.927</i>	25.63	0.915	24.20	0.916	23.98
Dreambooth + DoRA	<i>0.907</i>	24.11	<i>0.925</i>	22.18	0.924	<i>25.71</i>	<i>0.917</i>	24.28	<i>0.918</i>	24.05
Dreambooth + AdaLoRA	0.906	24.09	0.924	22.16	0.927	25.69	0.916	24.25	0.917	24.03
Dreambooth + SaRA	0.800	<b>26.37</b>	0.897	<i>23.91</i>	0.896	25.67	0.895	<b>25.90</b>	0.876	<i>25.52</i>
<b>Dreambooth + FeRA (Ours)</b>	<b>0.910</b>	<i>26.35</i>	<b>0.930</b>	<b>24.03</b>	<b>0.935</b>	<b>25.75</b>	<b>0.920</b>	<i>25.00</i>	<b>0.923</b>	<b>25.72</b>

Table 8. Inference-time comparison between LoRA and FeRA across multiple Stable Diffusion backbones. Values are relative per-step runtime (LoRA = 1.00).

Method	SD 1.5	SD 2.0	SD 3.0	SDXL	FLUX.1
LoRA (baseline)	1.00×	1.00×	1.00×	1.00×	1.00×
<b>FeRA (ours)</b>	1.12–1.20×	1.10–1.18×	1.08–1.15×	1.05–1.12×	1.04–1.10×